Sampling Pattern Augmentation to Enhance Deep Learning-based Image Reconstruction of MRI

Kazuki Yamato* and Satoshi Ito*
* Department of Fundamental Engineering, School of Engineering, Utsunomiya University
E-mail: {yamato, itohst}@is.utsunomiya-u.ac.jp Tel/Fax: +81-286896277

***Abstract*—The application of compressed sensing (CS) to MRI enables the acceleration of imaging times. CS can approximate an original signal from measurements that do not satisfy the sampling theorem. While CS can reduce the sampling time of k-space signals by reconstructing an MR image from limited measurement signals, there are still issues such as reconstruction time and optimal parameter search due to the CS optimization algorithm. In contrast, unrolling-based network models that can learn the parameters of the CS optimization algorithm to appropriate values for the subject are proposed, and the reconstruction performance is improved by applying the model to CS. However, the unrolling-based network models are trained based on a specific sampling pattern, and the reconstruction performance is adversely affected when the reconstruction is carried out using an untrained pattern. In this study, a sampling pattern augmentation method that employs multiple sampling patterns for learning is proposed as a means of developing a model that is not dependent on specific sampling patterns. Simulation experiments demonstrated that the reconstructed images using the sampling pattern augmentation exhibited superior quality compared to those reconstructed using conventional methods, while requiring a significantly shorter learning time. Moreover, it was confirmed that the proposed method yields high reconstruction performance even when reconstructing with untrained patterns.**

I. Introduction

Magnetic resonance imaging (MRI) is a non-invasive technique that can provide high-contrast cross-sectional images of the body. However, the requisite relaxation time for signal recovery results in imaging times that are typically between 20 and 60 minutes. Consequently, numerous researchers have explored avenues for accelerate MRI, including parallel imaging [1], [2] and compressed sensing [3], [4]. In recent years, the reconstruction of under-sampled k-space data obtained by compressed sensing using deep learning [5] has enabled the generation of high-quality images in a time-efficient manner, when compared to traditional iterative reconstruction methods.

The field of deep learning-based reconstruction methods can be divided into four principal categories. The first category comprises image domain-based methods [6]–[9], which employ an inverse Fourier transform (IFT) to the under-sampled signal in order to obtain an initial image, which serves as the primary input to the deep learning process. The second category comprises k-space based methods [10], in which an under-sampled signal is directly input to the deep learning model, and then IFT is applied to obtain the reconstructed image. However, methods belonging to this category have not been widely studied due to the potential for any artifacts introduced by the deep learning to be spread over the reconstructed image. The third category comprises iterative unrolling methods [11]–[14], which commence with an optimization problem whose solution is the image to be reconstructed. The optimization algorithm is then unrolled into the deep learning. Notably, the ADMM-Net proposed by Yang et al. [11] has relatively good reconstruction performance in the same category. The fourth category comprises methods that learn the image directly from an under-sampled signal [15]. This category typically necessitates the incorporation of fully connected layers, resulting in a network of considerable scale.

In the context of deep learning reconstruction methods, the generation of artifacts resulting from the under-sampling of k-space data, utilizing a specific sampling pattern, is addressed through the implementation of a learning process. This enables the removal of artifacts that may otherwise manifest in the reconstructed image. In other words, the characteristics of the artifacts that appear in the reconstructed image are different for sampling patterns not used in training, which makes effective artifact removal difficult. Liu et al. proposed a novel sampling pattern augmentation technique [8], [9], which employs a combination of multiple sampling patterns during training with the objective of enhancing robustness in the event of disagreement between sampling patterns. Models trained with different sampling patterns are capable of estimating and removing a diverse range of artifacts. In contrast, the network proposed by Liu et al. is based on image domain-based methods, including U-Net [16] and Generative Adversarial Networks (GANs) [17]. It thus appears that there is scope for further enhancement of reconstruction performance through the incorporation of sampling pattern augmentation into iterative unrolling models such as ADMM-Net.

In this paper, we introduce sampling pattern augmentation to ADMM-Net, which has particularly high reconstruction capability among iterative unrolling models, with the aim of developing a model that is robust to changes in sampling patterns. To validate the effectiveness of the proposed approach, we conducted experimental simulations in which image reconstruction with sampling pattern augmentation was compared with that without sampling pattern augmentation, i.e., using a single sampling pattern. The experimental outcomes demonstrate the effectiveness and utility of the sampling pattern augmentation, even in the context of iterative unrolling models.

II. Methods

A. ADMM-Net

Compressed sensing is a technique that allows the reconstruction of an original signal from fewer under-sampled signals than required by the Nyquist-Shannon sampling theorem, provided the target signal has sparsity. Thus, compressed sensing can accelerate MRI imaging time by under-sampling the Fourier transform imaging signals. The ADMM-Net proposed by Yang et al. was developed by using unrolling ADMM optimization [18], [19] to train the regularization parameters of compressed sensing. The reconstructed image ρ is estimated by solving the optimization problem as follows:

$$\hat{\boldsymbol{\rho}} = \arg\min_{\boldsymbol{\rho}} \left\{ \frac{1}{2}\|\mathbf{PF}\boldsymbol{\rho} - \mathbf{m}\|_2^2 + \sum_{l=1}^{L} \lambda_l g[\mathbf{D_l}\boldsymbol{\rho}] \right\}, \quad (1)$$

where $\mathbf{m}$ is an under-sampled signal, $\mathbf{P}$ is an under-sampling matrix, $\mathbf{F}$ is the Fourier transform, $\mathbf{D_l}$ is an undetermined linear transform, $g[\cdot]$ is a nonlinear regularization function, and λ_l is a regularization parameter.

By introducing the independent auxiliary variables $\mathbf{z} = \{\mathbf{z}_1, \mathbf{z}_2, \ldots, \mathbf{z}_L\}$ in the image domain and using the Lagrangian multiplier β, the iterations of the ADMM algorithm are represented as follows:

$$\begin{cases} \arg\min\limits_{\boldsymbol{\rho}} \frac{1}{2}\|\mathbf{PF}\boldsymbol{\rho} - \mathbf{m}\|_2^2 - \frac{r}{2}\|\boldsymbol{\rho} + \boldsymbol{\beta} - \mathbf{z}\|_2^2, \\ \arg\min\limits_{\mathbf{z}} \sum_{l=1}^{L} \lambda_l g(\mathbf{D}_l \mathbf{z}) + \frac{r}{2}\|\boldsymbol{\rho} + \boldsymbol{\beta} - \mathbf{z}\|_2^2, \\ \boldsymbol{\beta} \longleftarrow \boldsymbol{\beta} + \tilde{\eta}(\boldsymbol{\rho} - \mathbf{z}), \end{cases} \quad (2)$$

where the parameter $\tilde{\eta}$ is an update rate, and r is a penalty parameter. If $\mathbf{I}$ is a unit matrix, these iterations have the following solutions:

$$\begin{cases} \mathbf{R}^{(n)} : \boldsymbol{\rho}^{(n)} = \mathbf{F}^T \dfrac{\left[\mathbf{P}^T\mathbf{y} + r\mathbf{F}(\mathbf{z}^{(n-1)} - \boldsymbol{\beta}^{(n-1)})\right]}{(\mathbf{P}^T\mathbf{P} + r\mathbf{I})}, \\ \mathbf{Z}^{(n)} : \mathbf{z}^{(n,k)} = \mu_1 \mathbf{z}^{(n,k-1)} + \mu_2(\boldsymbol{\rho}^{(n)} + \boldsymbol{\beta}^{(n-1)}) \\ \qquad - \sum_{l=1}^{L} \lambda_l \mathbf{D}_l^T \mathcal{H}[\mathbf{D}_l \mathbf{z}^{(n,k-1)}], \\ \mathbf{M}^{(n)} : \boldsymbol{\beta}^{(n)} = \boldsymbol{\beta}^{(n-1)} + \tilde{\eta}(\boldsymbol{\rho}^{(n)} - \mathbf{z}^{(n)}), \end{cases} \quad (3)$$

where $\mathcal{H}[\cdot]$ denotes a non-linear transform corresponding to the gradient of the regularization function $g[\cdot]$, and k denotes the k-th sub-iteration of $\mathbf{z}^{(n)}$. In the solution $\mathbf{Z}$, $\mu_1 = 1 - \delta r$, $\mu_2 = \delta r$, $\lambda_l = \delta\lambda_l$ where δ is the gradient descent step size. As the ADMM algorithm iterates, the solutions represented in (3) are updated alternately in the order of $\mathbf{R}^{(n)}$, $\mathbf{Z}^{(n)}$, and $\mathbf{M}^{(n)}$.

Figure 1 shows the data-flow graph of ADMM-Net. As shown in Fig. 1, the n-th stage in the data-flow graph corresponds to the n-th iteration of the ADMM algorithm. In ADMM-Net, the solutions of (3), i.e. $\mathbf{R}$, $\mathbf{Z}$, and $\mathbf{M}$, act as three kinds of layers. The layers $\mathbf{R}$, $\mathbf{Z}$, and $\mathbf{M}$ are the reconstruction layer, the noise reduction layer, and the multiplier update layer, respectively, and a set of these layers is treated as a stage, which is equivalent to a solving step of the ADMM algorithm in (3). ADMM-Net trains the penalty parameter r in the reconstruction layers, the convolution filters of the two convolution layers, which are sub-layers of the noise reduction layers $\mathbf{Z}$, the multiplier update parameter $\tilde{\eta}$, and the regularization parameter λ_l.

In the training of ADMM-Net, under-sampled signals are input to the network, and the loss between the reconstructed image output from the network and the full-data image is calculated. The loss function of the ADMM-Net uses the normalized mean squared error (NMSE).

B. Sampling Pattern Augmentation

In general, deep learning reconstruction methods employ a single sampling pattern for model training. It is therefore challenging to obtain high-quality images from an under-sampled MR signal using an untrained sampling pattern. By augmenting the sampling patterns utilized in model training from a single pattern to multiple patterns as illustrated in Fig. 2, the constraint imposed by employing a single sampling pattern in deep learning reconstruction methods can be alleviated. In the sampling pattern augmentation process, a library containing N sampling patterns are generated, and a sampling pattern to be used for each image is randomly selected from the library. The selected pattern is reselected with each change in epoch. Accordingly, the number of sampling patterns in the library, designated as N, can be expressed as follows:

$$N = EI_{\mathrm{train}}, \quad (4)$$

where E and I_{train} represent the number of epochs in model training and the number of training images, respectively. In this paper, the generated sampling patterns are 1D Cartesian patterns sampled along the phase-encoding direction. Fig. 3 shows an example of the generated sampling patterns.

C. Experimental Configuration

To verify the effectiveness of the proposed method, we conducted experimental simulations. In this study, the robustness of the sampling pattern augmentation applied to the unrolling model is evaluated and its reconstruction performance is compared with that of the image domain-based model. In the experiments, ADMM-Net is used as the unrolling model method and U-net is used as the image domain-based model, and 485 T1-weighted MR images of the heads of consenting volunteers from IXI Dataset [20] were used. 400 randomly selected images were used for training and the rest were for testing. All images were 256×256 pixels.

In the configurations of ADMM-Net, the number of epochs, the number of stages, the number of convolution filters, filter size, the activation function, optimizer, and learning rate were set to 300, 10, 64, 5×5, Rectified Linear Unit (ReLU) [21], Adam [22], and 10^{-3}, respectively. In the configurations of U-Net, the following parameters were set: the number of epochs, the number of stages, the number of initial convolution filters, filter size, the activation function , optimizer, and learning rate. These were set to 300, 5, 64, 3×3, ReLU, Adam, 10^{-4},

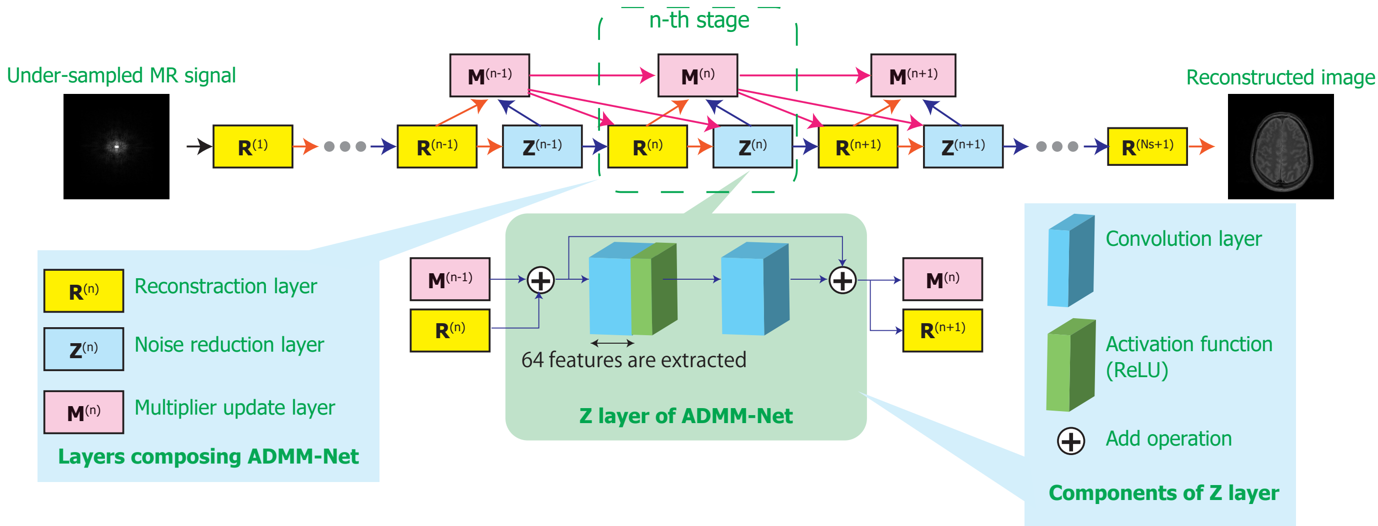

Fig. 1. The data flow graph for ADMM-Net. ADMM-Net comprises three distinct types of layers: the reconstruction layer, the noise reduction layer, and the multiplier update layer. The noise reduction layer comprises two convolution layers and an activation layer situated between them.

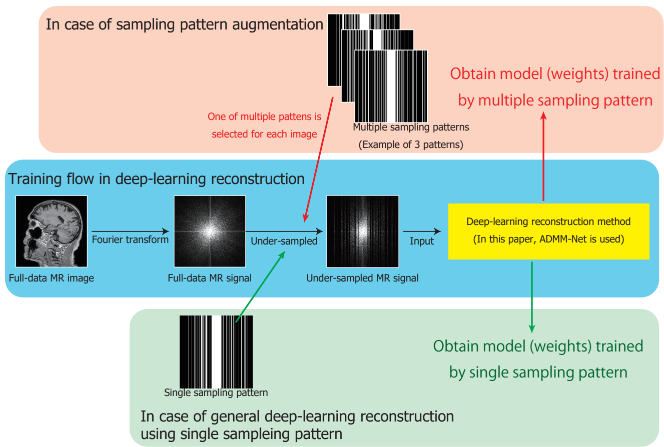

Fig. 2. Training flow of deep-learning reconstruction when under-sampling with single sampling pattern and the sampling pattern augmentation.

respectively. Furthermore, the reconstructed images by U-Net are subjected to the data consistency (DC), thereby improving the quality of the reconstructed images. The reconstructed image is then subjected to a calculation of the data consistency, denoted as $\boldsymbol{\rho}_{DC}$, as follows:

$$\boldsymbol{\rho}_{\mathrm{DC}} = \mathbf{F}^{T}[\mathbf{Pm} + (\mathbf{I} - \mathbf{P})\mathbf{F}\boldsymbol{\rho}_{\mathrm{U-Net}}] \tag{5}$$

where $\boldsymbol{\rho}_{U-Net}$ represents a reconstructed image by U-Net. $\mathbf{F}$, $\mathbf{P}$, and $\mathbf{I}$ represent the Fourier transform, a sampling pattern matrix, and a unit matrix, respectively. $\mathbf{m}$ represent the under-sampled MR signal. Therefore, the quality of the reconstructed images can be enhanced by replacing the under-sampled points of the MR signal of $\boldsymbol{\rho}_{U-Net}$ with $\mathbf{Pm}$.

The number of sampling patterns contained in the sampling pattern library are $400 \times 300 = 120000$. The sampling patterns used in the experiments are based on a Gaussian distribution. The standard deviation of the Gaussian distribution σ is as

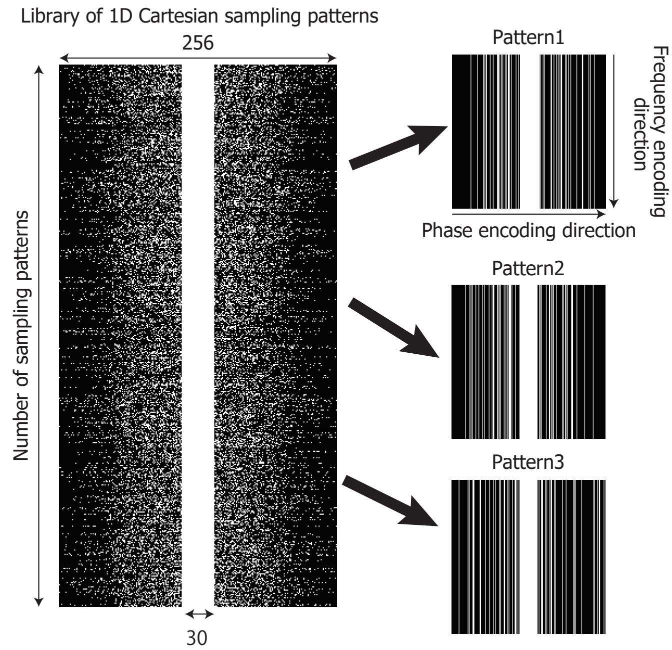

Fig. 3. Example of the 1D variable density Cartesian random sampling patterns. In this example, the matrix size of sampling patterns is set to 256×256. The White regions of the library and Pattern 1 to 3 represent under-sampling points of MR signal, and black regions are zero-filling points.

follows:

$$\sigma = 256\alpha, \tag{6}$$

where α denotes a parameter that controls the distribution of under-sampled MR signals by the sampling pattern. In addition, the low-frequency components are sampled continuously because the MR signals have a high energy concentration in the low-frequency component. The number of continuous sampling points in the

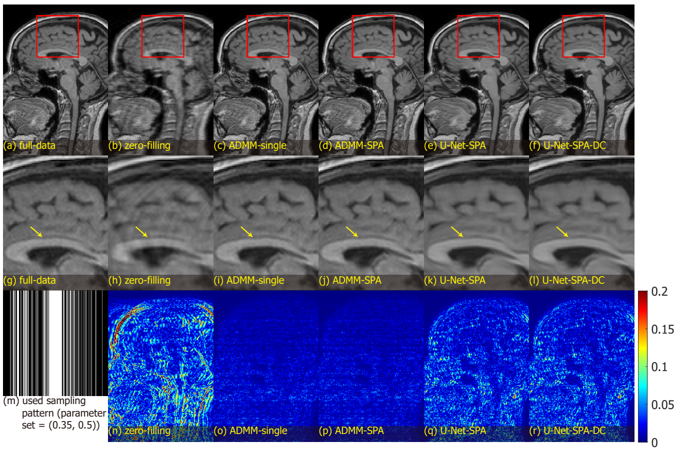

Fig. 4. Reconstructed images by each reconstruction method. The images were reconstructed from the under-sampled MR signal in accordance with a sampling pattern that had not been trained, as shown in (m). (g)-(l) show enlarged views of the red rectangle areas in (a)-(f), respectively. (n)-(r) are the error maps between the full-data and each reconstructed images. (c) was reconstructed by the model that had been trained with a sampling pattern of $(R, \alpha) = (0.3, 0.5)$. In (d)-(f), the sampling pattern augmentation (SPA) is employed.

experiments is set to 30. The sampling patterns used for the sampling pattern augmentation is generated by setting the sampling rate R and α. In the experiments, R and α are considered as a parameter set, and the sampling patterns are generated from 5 parameter sets, i.e., $(R, \alpha) \in \{(0.2, 0.5), (0.3, 0.3), (0.3, 0.5), (0.3, 0.8), (0.4, 0.5)\}$. Note that the signal sampling points are determined randomly.

To evaluate the robustness, the proposed model using the sampling pattern augmentation in ADMM-Net and the conventional model trained with a single pattern were tested by generating 10 different sampling patterns for testing with the parameter set used in single pattern learning. As an example, when the single pattern learning model using the parameter set $(0.2, 0.5)$ is tested, 10 sampling patterns for testing are generated with the parameter set $(0.2, 0.5)$.

The quantitative evaluation of the reconstructed images was conducted using three metrics: the Peak Signal-to-Noise Ratio (PSNR) and the Learned Perceptual Image Patch Similarity (LPIPS) metric [23]. The LPIPS employs pre-trained image feature extraction networks comprising comvolutional neural network (CNN)-based models such as AlexNet [24] and VGG [25]. The LPIPS metric, which employs a pre-trained AlexNet model available on GitHub, was used to assess the results of the experiments. It should be noted that a lower value of the LPIPS indicates a higher quality of reconstructed images.

The experimental simulations were performed on a computer with an Intel(R) Core(TM) i9-11900K (3.5 GHz), with 64.0 GB of RAM, and NVIDIA GeForce RTX 3090 GPU running Windows 10. The software used was Python 3.9.5, PyTorch 2.3.1, and CUDA ToolKit 12.1.

III. Experimental results

Figure 4 shows the reconstructed images when the untrained sampling pattern is used for the reconstruction. Fig. 4(m) shows the used sampling pattern in this experiment, whose sampling rate and a parameter α are set to 0.35 and 0.5, respectively. Table I shows the quantitative evaluation results of the reconstructed images. In the image reconstruction using ADMM-Net, a comparison of the reconstruction results with and without the sampling pattern augmentation indicates that the image reconstructed by the model with the sampling pattern augmentation is more accurate reproducing the indicated texture by the arrows than the image reconstructed by the model trained with a single sampling pattern. As shown in the quantitative evaluation results, the reconstructed images with the sampling pattern augmentation have higher PSNR than those of the single pattern model. On the other hand, the LPIPS of the reconstructed images with the sampling pattern augmentation was equal or higher for $(R, \alpha) = (0.2, 0.5)$ and $(0.35, 0.5)$, but lower for $(R, \alpha) = (0.3, 0.5)$ and $(0.4, 0.5)$ than that of the model trained with the single sampling pattern.

Subsequently, a comparison is conducted between ADMM-Net and U-Net, with the sampling pattern augmentation. As shown in Fig. 4, the reconstructed image by U-Net with the sampling pattern augmentation exhibits a notable degree of smoothing and a discernible loss of detail structure. Notwithstanding the enhancement of the reconstructed image quality through data consistency, no significant improvements were observed. In contrast, the ADMM-Net with the sampling pattern augmentation demonstrated superior performance in preserving detail structure compared to U-Net. As shown in the quantitative evaluation, the evaluation metrics of ADMM-Net with the sampling pattern augmentation exhibited better than those of U-Net.

IV. Discussion

In the sampling pattern augmentation conducted in the experiments, 120,000 different sampling patterns were used for model training. This equates to 120,000 artifacts being learned, with the model parameters optimized to remove these artifacts. It is therefore hypothesised that the application of sampling pattern augmentation improves the image quality of the reconstructed images both quantitatively and qualitatively.

From Fig. 4 and Table I, ADMM-Net with the sampling pattern augmentation has better reconstruction performance than that of using a single sampling pattern in terms of PSNR. In the experiments, model training is performed with 300 epochs, and the model whose reconstructed image quality is the highest among the 300 models is selected as the model for testing. The metric that determines the model for testing is PSNR. In other words, the models are determined such that both the sampling pattern augmentation and the single sampling pattern have the maximum PSNR of the reconstructed images. In addition, the loss functions of ADMM-Net and U-Net are NMSE and MSE, and the PSNR formula includes MSE. Therefore, the changes in MSE directly affect the changes in PSNR. Evaluation by

TABLE I
QUANTITATIVE METRICS COMPARING THE FULL-DATA IMAGES.

(R, α)	(0.2, 0.5)		(0.3, 0.5)		(0.4, 0.5)		(0.35, 0.5)	
	PSNR [dB]	LPIPS	PSNR [dB]	LPIPS	PSNR [dB]	LPIPS	PSNR [dB]	LPIPS
ADMM-Net (SPA)	29.02±0.71	0.016±0.008	34.07±0.93	0.016±0.003	37.37±1.13	0.012±0.002	35.74±0.99	0.007±0.002
ADMM-Net (single)	28.90±0.65	0.038±0.007	33.92±0.97	0.011±0.003	37.22±1.23	0.005±0.002	35.52±1.02	0.007±0.002
U-Net (SPA)	28.06±0.65	0.058±0.011	29.49±0.60	0.045±0.008	30.36±0.59	0.035±0.007	30.03±0.58	0.038±0.007
U-Net (SPA) + DC	28.92±0.67	0.052±0.011	31.32±0.61	0.035±0.008	32.98±0.58	0.024±0.006	32.26±0.59	0.028±0.007

TABLE II
COMPUTATIONAL COMPLEXITY

	Training [min]	Reconstruction [ms]	Parameters
ADMM-Net (SPA)	24.80	3.59	33,823
ADMM-Net (single)	24.80	3.81	33,823
U-Net (SPA)	32.21	725.54	22,023,937

PSNR has a high affinity with the loss functions such as NMSE and MSE. As a result, the effectiveness of the sampling pattern augmentation could be demonstrated in terms of PSNR.

On the other hand, ADMM-Net with the sampling pattern augmentation exhibits suboptimal performance with respect to the LPIPS metric. The LPIPS metric can be evaluated in accordance with human perceptual characteristics. In particular, LPIPS tends to evaluate more highly an image in which random noise-like artifacts remain but the detailed structure has been restored than an image in which the detailed structure has been destroyed by smoothing through reconstruction. In contrast, PSNR is evaluated more highly when the error between the pixel values of the full data and those of the reconstructed image is small. Consequently, the evaluation is higher even if smoothing or blurring has occurred. As previously stated, since the selection criterion for the test model was PSNR, LPIPS of the reconstructed image was not necessarily highly evaluated. Therefore, the evaluation when LPIPS is used as the model selection criterion is a future issue.

Table II shows the processing times for training and reconstruction, as well as the number of parameters associated with each model. As shown in the table, it is clear that the training time, reconstruction time, and number of parameters remain unaltered when the sampling pattern augmentation is introduced or excluded. In the sampling pattern augmentation, a sampling pattern for each image is randomly selected from the sampling pattern library and reselected with each change in epoch. In other words, the number of training data remains constant, in contrast to the data augmentation approach. Furthermore, the sampling pattern augmentation is a form of preprocessing that occurs before the network input for training. Therefore, the number of parameters comprising the model remains unaltered in the presence or absence of the sampling pattern augmentation.

With regard to the issue of computational complexity, it can be observed that the reconstruction of ADMM-Net is capable of begin carried out at a speed that is 190 times faster than that of U-Net. The U-Net model comprises a multitude of convolution layers, with a total of 650 times more parameters than those comprising the ADMM-Net model. Therefore, ADMM-Net demonstrated superior performance in terms of both speed and image quality compared to U-Net.

In this paper, the experiments were performed on real-valued images, but the images acquired from MRI are complex images with phase components. From practical point of view, it is necessary to confirm the effectiveness of sampling pattern expansion also for complex images, and this is a topic for future work.

V. CONCLUSIONS

In this study, we introduced the sampling pattern augmentation to an iterative unrolling model, specifically ADMM-Net in order to enhance the robustness of the trained model in the presence of sampling pattern discrepancies. In the sampling pattern augmentation, a sampling pattern for each image is randomly selected from the sampling pattern library and reselected with each change in epoch. To verify the effectiveness of the sampling pattern augmentation in enhancing the robustness of the trained model, image reconstruction experiments were conducted using untrained sampling patterns. As a consequence, the reconstructed images produced by ADMM-Net with the sampling pattern augmentation exhibited a higher PSNR than those of the model trained with a single sampling pattern. In comparison to the image domain-based model, i.e., U-Net, with the sampling pattern augmentation, it was confirmed that ADMM-Net with the sampling pattern augmentation exhibited superior performance in terms of reconstruction speed and quality relative to U-Net.

ACKNOWLEDGMENT

This work was supported by a Grant for Young Exploratory Research in the School of Engineering, Utsunomiya University. The authors thank the Information eXtraction from Images project for creating the IXI Dataset.

REFERENCES

[1] D. Liang, B. Liu, J. Wang, and L. Ying, "Accelerating sense using compressed sensing," *Magnetic Resonance in Medicine*, vol. 62, no. 6, pp. 1574–1584, 2009.

[2] H. Jung, K. Sung, K. S. Nayak, E. Y. Kim, and J. C. Ye, "K-t focuss: A general compressed sensing framework for high resolution dynamic mri," *Magnetic Resonance in Medicine*, vol. 61, no. 1, pp. 103–116, 2009.

[3] D. Donoho, "Compressed sensing," *IEEE Transactions on Information Theory*, vol. 52, no. 4, pp. 1289–1306, 2006. DOI: 10.1109/TIT.2006.871582.

[4] M. Lustig *et al.*, "Sparse mri: The application of compressed sensing for rapid mr imaging," *Magnetic Resonance in Medicine*, vol. 58, no. 6, pp. 1182–1195, 2007. DOI: https://doi.org/10.1002/mrm.21391.

[5] S. Wang, Z. Su, L. Ying, *et al.*, "Accelerating magnetic resonance imaging via deep learning," in *2016 IEEE 13th International Symposium on Biomedical Imaging (ISBI)*, 2016, pp. 514–517. DOI: 10.1109/ISBI.2016.7493320.

[6] G. Yang, S. Yu, H. Dong, *et al.*, "Dagan: Deep de-aliasing generative adversarial networks for fast compressed sensing mri reconstruction," *IEEE Transactions on Medical Imaging*, vol. 37, no. 6, pp. 1310–1321, 2018. DOI: 10.1109/TMI.2017.2785879.

[7] M. Mardani, E. Gong, J. Y. Cheng, *et al.*, "Deep generative adversarial neural networks for compressive sensing mri," *IEEE Transactions on Medical Imaging*, vol. 38, no. 1, pp. 167–179, 2019. DOI: 10.1109/TMI.2018.2858752.

[8] F. Liu, L. Feng, and R. Kijowski, "Mantis: Model-augmented neural network with incoherent k-space sampling for efficient mr parameter mapping," *Magnetic Resonance in Medicine*, vol. 82, no. 1, pp. 174–188, 2019. DOI: https://doi.org/10.1002/mrm.27707.

[9] F. Liu, A. Samsonov, L. Chen, R. Kijowski, and L. Feng, "Santis: Sampling-augmented neural network with incoherent structure for mr image reconstruction," *Magnetic Resonance in Medicine*, vol. 82, no. 5, pp. 1890–1904, 2019. DOI: https://doi.org/10.1002/mrm.27827.

[10] Y. Han, L. Sunwoo, and J. C. Ye, "k -space deep learning for accelerated mri," *IEEE Transactions on Medical Imaging*, vol. 39, no. 2, pp. 377–386, 2020. DOI: 10.1109/TMI.2019.2927101.

[11] Y. Yang *et al.*, "Admm-csnet: A deep learning approach for image compressive sensing," *IEEE Transactions on Pattern Analysis and Machine Intelligence*, vol. 42, no. 3, pp. 521–538, 2020. DOI: 10.1109/TPAMI.2018.2883941.

[12] K. Hammernik *et al.*, "Learning a variational network for reconstruction of accelerated mri data," *Magnetic Resonance in Medicine*, vol. 79, no. 6, pp. 3055–3071, 2018. DOI: https://doi.org/10.1002/mrm.26977.

[13] J. Zhang and B. Ghanem, "Ista-net: Interpretable optimization-inspired deep network for image compressive sensing," in *Proceedings of the IEEE Conference on Computer Vision and Pattern Recognition (CVPR)*, Jun. 2018.

[14] H. K. Aggarwal *et al.*, "Modl: Model-based deep learning architecture for inverse problems," *IEEE Transactions on Medical Imaging*, vol. 38, no. 2, pp. 394–405, 2019. DOI: 10.1109/TMI.2018.2865356.

[15] B. Zhu, J. Z. Liu, S. F. Cauley, B. R. Rosen, and M. S. Rosen, "Image reconstruction by domain-transform manifold learning," *Nature*, vol. 555, no. 7697, pp. 487–492, 2018.

[16] O. Ronneberger, P. Fischer, and T. Brox, "U-net: Convolutional networks for biomedical image segmentation," in *Medical Image Computing and Computer-Assisted Intervention–MICCAI 2015: 18th International Conference, Munich, Germany, October 5-9, 2015, Proceedings, Part III 18*, Springer, 2015, pp. 234–241.

[17] I. Goodfellow, J. Pouget-Abadie, M. Mirza, *et al.*, "Generative adversarial networks," *Communications of the ACM*, vol. 63, no. 11, pp. 139–144, 2020.

[18] "A dual algorithm for the solution of nonlinear variational problems via finite element approximation," *Computers Mathematics with Applications*, vol. 2, no. 1, pp. 17–40, 1976, ISSN: 0898-1221. DOI: https://doi.org/10.1016/0898-1221(76)90003-1.

[19] J. Eckstein and D. P. Bertsekas, "On the douglas—rachford splitting method and the proximal point algorithm for maximal monotone operators," *Mathematical Programming*, vol. 55, no. 1, pp. 293–318, Apr. 1992. DOI: 10.1007/BF01581204.

[20] *IXI dataset*, https://brain-development.org/ixi-dataset/(Accessed: July 16, 2024).

[21] V. Nair and G. E. Hinton, "Rectified linear units improve restricted boltzmann machines," in *Proceedings of the 27th international conference on machine learning (ICML-10)*, 2010, pp. 807–814.

[22] D. P. Kingma and J. Ba, "Adam: A method for stochastic optimization," *arXiv preprint arXiv:1412.6980*, 2014.

[23] R. Zhang, P. Isola, A. A. Efros, E. Shechtman, and O. Wang, "The unreasonable effectiveness of deep features as a perceptual metric," in *Proceedings of the IEEE Conference on Computer Vision and Pattern Recognition (CVPR)*, Jun. 2018.

[24] A. Krizhevsky, I. Sutskever, and G. E. Hinton, "Imagenet classification with deep convolutional neural networks," in *Advances in Neural Information Processing Systems*, F. Pereira, C. Burges, L. Bottou, and K. Weinberger, Eds., vol. 25, Curran Associates, Inc., 2012.

[25] K. Simonyan and A. Zisserman, "Very deep convolutional networks for large-scale image recognition," *CoRR*, vol. abs/1409.1556, 2014.